Inconel 625 Coatings on AISI 304 Steel using Laser Cladding: Microstructure and Hardness

Vadakke Parambil Vijeesh
Department of Mechanical Engineering, National Institute of Technology Karnataka, India
vijeesh@nitgoa.ac.in (corresponding author)

Motagondanahalli Rangarasaiah Ramesh
Department of Mechanical Engineering, National Institute of Technology Karnataka, India
rameshmr@nitk.edu.in

Aroor Dinesh Anoop
Mechanical Engineering Department, National Institute of Technology Goa, India
anoop@nitgoa.ac.in

Received: 21 August 2023 | Revised: 11 September 2023 | Accepted: 14 September 2023

 DOI: https://doi.org/10.48084/etasr.6297

ABSTRACT

Nickel-base super alloys such as Inconel 625 are preferred in high-temperature and corrosive environments. Since Inconel 625 is expensive and often difficult to machine, it is advantageous to deposit a protective coating of this alloy on a less costly and easily machinable substrate material such as stainless steel. In the present work, coatings were produced on AISI 304 steel substrate by depositing Inconel 625 powder using the laser cladding technique. As-received powder particles of Inconel 625 alloy were characterized using X-Ray Diffraction (XRD) and Field Emission Scanning Electron Microscopy (FESEM). After laser cladding, it becomes important to carry out the microstructural analysis of the cross-sectional areas of the coating and the substrate/coating interface region, for further understanding of the structure-property correlations. In this study, the microstructural features of the coatings and substrate/coating interface were examined using an FESEM equipped with X-ray elemental analysis. The phase analysis of the coating was carried out using XRD. In the coating region, the growth of planar, cellular, columnar dendritic, and equiaxed grains was noticed. It was observed that small amounts of Laves phase were precipitated. Furthermore, the laser-clad Inconel 625 coating showed superior microhardness over the stainless steel substrate.

Keywords-laser cladding; Inconel 625; super alloy; AISI 304; microstructure; microhardness

I. INTRODUCTION

Various industrial applications demand joining of dissimilar materials. Coatings of superalloys onto austenitic stainless steels find relevance in chemical process plants, oil, and gas industries [1]. Functional materials play a crucial role by imparting a range of properties to material components. These properties cannot be achieved through a single material alone, especially for long-lasting requirements [2]. Conventional coating methods such as surface welding and plasma spraying exhibit a few shortcomings. These techniques are slow, tough to automate, labor intensive, and require more heat input [3]. High heat input leads to problems such as distortion, embrittlement, and dimensional instability. On the other hand, additive manufacturing techniques are popular nowadays. Laser cladding is one such technique which imparts lower levels of dilution and distortion [4]. In the laser cladding technique, a laser beam melts both the additive material and a thin layer of the substrate, ensuring a metallurgical bonding between them. The additive alloy may be introduced in-situ into the interaction zone of the laser beam and the substrate, either in wire or in powder form. In recent years, a few studies have been conducted to investigate the laser cladding of superalloy coatings on stainless steel base. Authors in [5] compared the performances of a Nd:YAG laser and a Yb:YAG monomode fiber laser source by generating the cladding tracks of cobalt-base superalloy on AISI 304 stainless steel substrate. Authors in [6] explored how varying laser metal deposition parameters, including focal length, frequency, and scanning speed, influence the characteristics of cobalt-base superalloy deposited onto precipitation-hardened martensitic stainless steel. Authors in [7] noted that the quality of the cladding layer is contingent on the following factors, ranked in decreasing order of significance: scanning speed, power, and overlapping rate. Authors in [8-10] studied the dry friction, wear, and high temperature oxidation behavior of the laser cladding coatings produced using feedstock powders of nickel-base and cobalt-base superalloys onto a cold rolled stainless steel substrate.

Authors in [11] developed a laser cladded surface by using preplaced TiC powder which produced a remarkable increase in hardness and wear resistance in the cladded region. Authors in [12] evaluated the optimum laser processing parameters for deposition of defect-free cobalt-base superalloy cladding layer with suitable geometry (width, height, undulation, and dilution) on austenitic stainless steel. Authors in [13] implemented an online monitoring system to observe the rapid heating and cooling rates occurring during the laser cladding of nickel-base superalloy onto AISI 304 austenitic steel.

Limited literature exists about microstructural and mechanical investigations of superalloy layers fabricated via laser cladding on stainless steel substrate. The present work deals with the deposition of Inconel 625 powder, a nickel-base superalloy, on AISI 304 stainless steel using the laser cladding technique. This paper describes the clad layer microstructure, phase composition, and microhardness as functions of position. The findings from this study are pivotal for advancing the investigation into the viability of Inconel 625 claddings on stainless steel piston rings, aiming to improve their longevity.

II. MATERIALS AND METHODS

In the present study, AISI 304 austenitic stainless steel substrates with 10 mm diameter and 25 mm thickness were prepared for depositing the clads. Prior to the cladding process, the substrate surface was polished with sandpaper and cleaned with acetone to eliminate stains and other contaminants. A commercial, inert gas atomized Inconel 625 powder was used as the feedstock material for laser cladding. The nominal chemical composition of the substrate and the feedstock powder is given in Table I. Figure 1(a) displays the Field Emission Scanning Electron Microscopy (FESEM) image of the as-received Inconel 625 powder. It was observed that the majority of the powder particles were spherical in shape. However, few particles had small satellites attached. Image analysis of secondary electron micrographs revealed that the average size of the powder particle was approximately 70.4 μm (Figure 1(b)).

TABLE I. CHEMICAL COMPOSITION OF AISI 304 STEEL AND INCONEL 625 POWDER

Element (wt. %)	C	Si	Cr	Mn	Nb	Mo	Ni	Fe
AISI 304	0.05	0.4	20.01	1.17			7.97	70.4
Inconel 625	0.03	0.35	22.5	0.4	3.9	7.92	62.4	2.5

Laser cladding process was performed using an Yb-fiber laser system (IPG YLS-4000). The power and scanning velocity of the continuous wave laser beam were set at 1.5 kW and 10 mm/s, respectively. The diameter of the laser beam was fixed at 2.5 mm. During the cladding process, to provide a protective atmosphere, Argon gas was used with an injection rate of 18 l/min. The system utilized a coaxial type powder feeder nozzle. Clad powder was deposited onto the substrate at a feed rate of 360 mg/s. Argon was also utilized as powder carrier gas. Figure 2(a) shows the laser powder deposition system and the specimen setup. The entire arrangement was connected to a Computer Numerical Control (CNC) platform to achieve precision coating. The powder focus was 17 mm beneath the nozzle tip. The bidirectional scanning pattern was adopted with constant offset distance. The coaxial nozzle and the cladding procedure can be better understood with the help of the schematic diagram given in Figure 2(b). A homogeneous powder stream was ensured by the coaxial nozzle. Figure 2(c) shows the clad coated sample. The clad coating thickness achieved was about 1.6 mm using single-layer powder deposition with a 40% overlapping ratio. The average surface roughness of the laser-cladded surface was measured to be 28.3 μm.

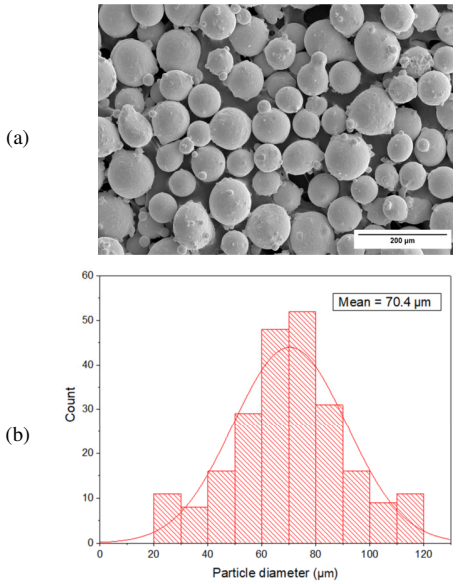

Fig. 1. Inconel 625 superalloy powder: (a) FESEM image, (b) particle size distribution estimated using the ImageJ software.

The laser cladded sample was sectioned using wire electric discharge machining to examine the evolution of microstructure along the coating depth. The cut section was polished with sandpapers down to 3000 grit size, followed by final polishing with a velvet cloth with alumina powder and diamond paste. The polished sample was chemically etched in aqua regia solution (3 ml HCl and 1 ml HNO_3) for 30 s. The microstructural morphology, as well as the elemental composition of the clad coatings were analyzed using a FEI Quanta FEG 250 field emission scanning electron microscope equipped with an Energy Dispersive Spectroscopy (EDS). A Bruker D8 Advance X-ray diffractometer was used in order to identify the phases present in the clad samples. The X-ray wavelength was 1.5406 Å using a Cu target source, while the scanning speed and step size were 2.8°/minute and 0.02°, respectively. A microhardness tester, Chennai Metco Economet VH-1 MDX, was utilized to obtain a Vickers microhardness profile along the cross section of the cladded sample. A load of 0.3 kg and a dwell time of 15 s were considered.

III. RESULTS AND DISCUSSION

A. Microstructure and Phase Analysis

The interaction between the laser beam, the additive alloy, and the substrate material results in complex metallurgical and solidification processes. The process variables such as laser

power, beam spot size, laser scanning velocity, laser beam absorption, and powder feed rate decide the temperature distributions in the melt pool. Within the melt pool, high temperature gradients induce intense convection due to the Marangoni effect [14, 15]. According to the Marangoni flow, the flow velocity is higher at the edge of the melt pool than that at the center. Also, the flow velocity at the bottom of the melt pool is higher than that at the top. The Marangoni effect leads to rapid homogenization of the melt. The cooling rates are very high during the laser cladding process due to which solid-state diffusive transformations are usually inhibited. Therefore, microstructural evolution is dependent on the solidification rate (R) and temperature gradient at the solid-liquid interface (G) [16].

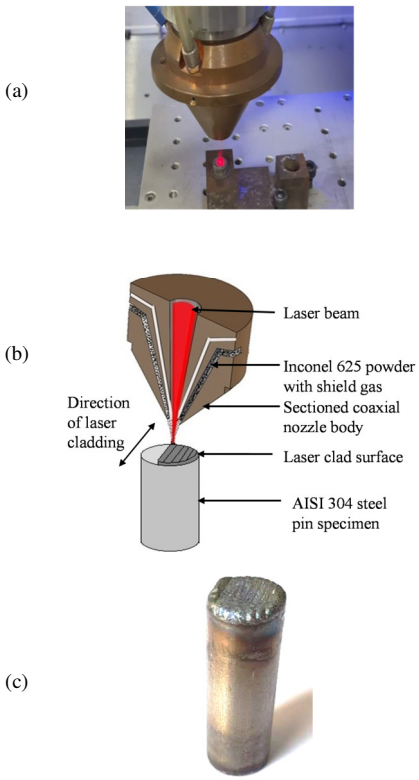

Fig. 2. Laser cladding process: (a) experimental arrangement, (b) schematic diagram of the coaxial powder deposition system, and (c) a laser cladded sample.

Figure 3 shows the secondary electron images of the laser clad layer and the interface region. The various grain morphology transformations observed throughout the cross-sectional area of the coating are due to the combined effects of G and R. This could be elucidated with the help of the solidification behavior of the melt pool [17]. While the ratio G/R governs the morphology preference of solidification structure, the product G×R, termed as cooling rate, decides the solidification microstructure size. From Figure 3, it is observed that the solidification began by epitaxial growth on the substrate. Due to the high value of G/R (constitutional undercooling criterion) at the bottom of the melt pool, few planar crystals appeared firstly, as shown in Figure 3(b). The formation of the region of plane fine grains indicated that the metallurgical bonding between the substrate and the clad layer is of high strength [18]. Cracks or pores have not been found in the coating/substrate interface. With the solidification progression, the value of G/R decreased. Simultaneously, the cooling rate increased from zero at bottom of the layer to a maximum value at the top of the coating. As the solid/liquid interface shifted, the solidification structure changed from planar to cellular (Figure 3(b)) on account of the decreasing G and the enhancing R. In the middle zone of the coating, further reduction of G resulted in columnar dendritic structure (with primary and secondary dendritic arms) along the direction of G, as shown in Figure 3(c). Due to the very low G and the increased degree of constitutional supercooling, the solidification mode transitioned to equiaxed grains in the top zone of the coating, as displayed in Figure 3(d).

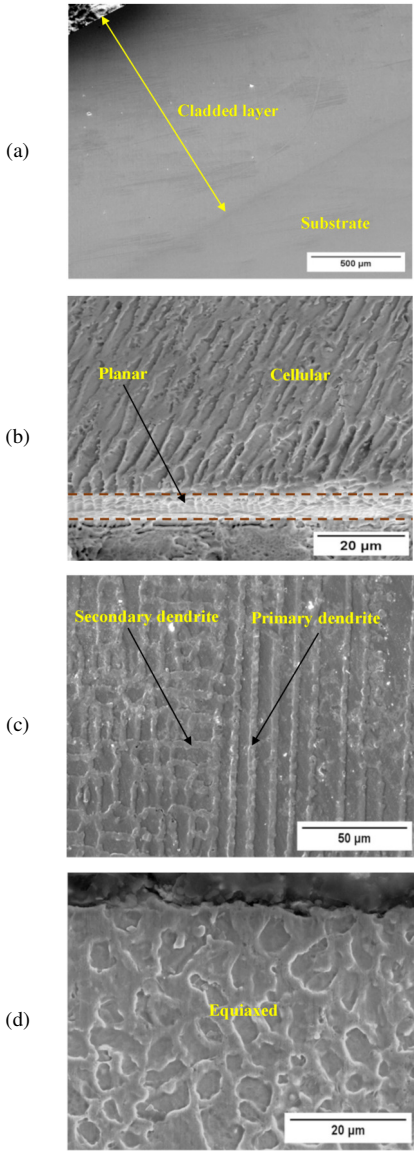

Fig. 3. FESEM images of a laser cladded sample: (a) cross-sectional, (b) coating/substrate interface zone, (c) middle, and (d) top zone of coating.

Figure 4 shows the EDS spot analysis results at different locations on the specimen cross-section. Figure 5 depicts the EDS elemental distribution maps near the clad/substrate interface.

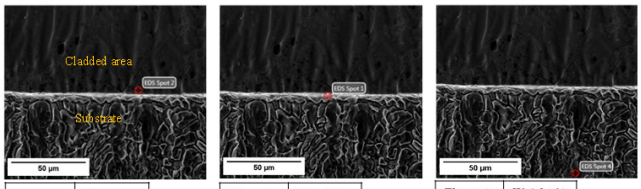

Elements	Weight %
Fe K	50.0
Ni K	25.3
Cr K	20.8

(a)

Elements	Weight %
Fe K	58.4
Ni K	5.1
Cr K	27.1

(b)

Elements	Weight %
Fe K	70.5
Ni K	7.7
Cr K	19.6

(c)

Fig. 4. FESEM-EDS spot analyses of a laser cladded sample: (a) clad region near the interface, (b) interface, (c) substrate.

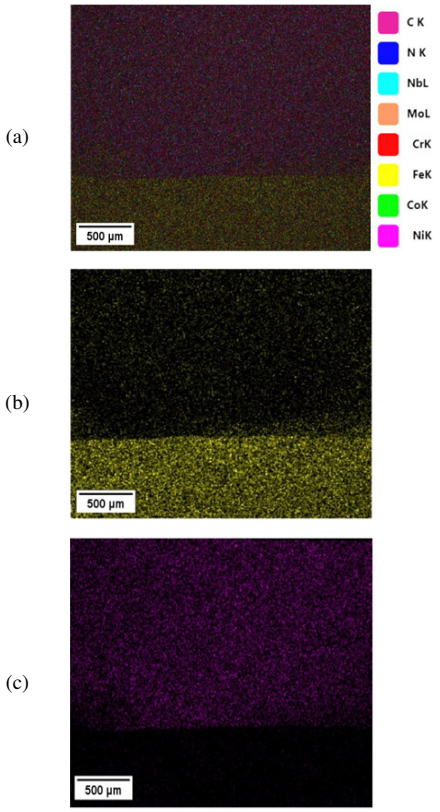

(a)

(b)

(c)

Fig. 5. EDS mappings around the clad/substrate interface: (a) existing elements, (b) Fe, (c) Ni.

It can be seen from Figure 4(c) that the Fe, Cr, and Ni contents in the substrate are consistent with the nominal composition of AISI 304 steel (see Table I). The Fe content in the coating (58.4 wt. % for white fusion zone and 50 wt.% for the clad region near the interface) increased significantly when compared with that of the additive alloy (2.5 wt.%), due to the dilution of Fe from the substrate into the coating. It is to be noted that the bulk composition of the substrate is Fe. Increase in Fe concentration in the transition region between the cladding layer and the substrate can be seen in Figure 5(b). The concentration of Ni is diminished in the region where Fe is enriched, as seen in Figures 4(a), 4(b), and 5(c). Similar observations were reported in [19].

Figure 6 displays the XRD patterns of the Inconel 625 powder and the Inconel 625 laser coating. For both samples, the major XRD peaks can be noticed at 2θ = 43.6°, 50.6°, and 74.6°. These are very comparable to the peak positions of pure Ni, as available from the JCPDS standard, present at 2θ = 44.5°, 51.9°, and 76.4°. Alloying and other trace elements in the solid solution of Inconel 625 affected the inter-planar spacing of the fcc-Ni present in the Inconel 625 [20]. Consequently, a slight difference occurred between the peak positions of pure Ni and the XRD peak positions of the Inconel 625.

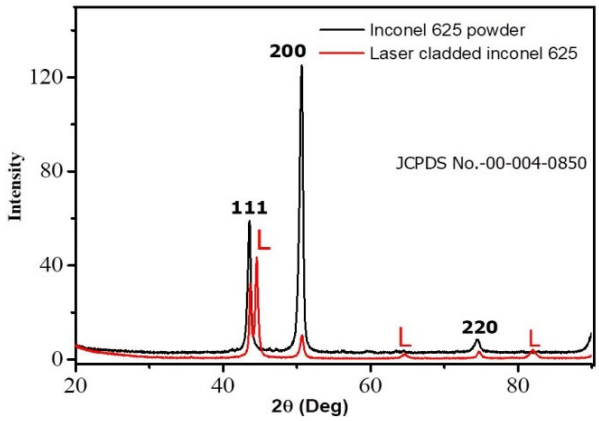

Fig. 6. XRD spectra of Inconel 625 powder and the laser cladded coating. L denotes the Laves phase.

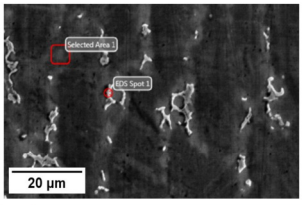

(a)

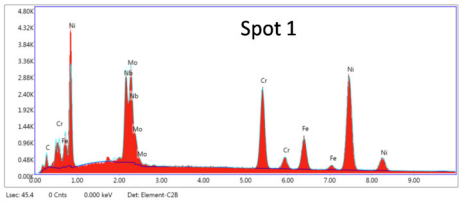

Elements	Weight %
Nb L	16.2
Mo L	11.9
Cr K	18.0
Fe K	9.4
Ni K	40

(b)

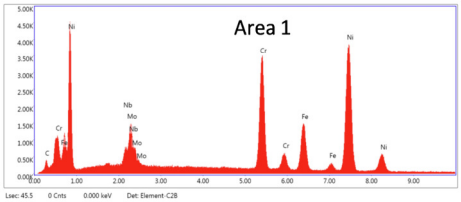

Elements	Weight %
Nb L	3.0
Mo L	6.3
Cr K	23.5
Fe K	13.4
Ni K	52.2

(c)

Fig. 7. (a) FESEM image showing Laves phases in the cladding layer, (b) EDS analysis of Laves phase, (c) EDS analysis of coating matrix phase.

As is evident from Figure 6, the Laves phase structure also appeared in the laser clad layer. However, the presence of the Laves phase was limited to a small region of the clad layer. Figure 7(a) shows the FESEM image of the Laves phases. The results of the EDS analysis revealed that the Laves phase contained more concentrations of Nb and Mo elements, and lesser Ni, Cr, and Fe elements (se Figure 7(b)) than the coating matrix phase (Figure 7(c)). Due to the reduced solid solubility of Mo and Nb elements in the fcc-Ni matrix, these alloying elements were rejected into the bulk liquid. During the solidification process, microsegregation of Nb and Mo into the interdendritic region resulted in the formation of Laves phases [21, 22]. The brittle nature of the Laves phase is detrimental to the mechanical properties [23].

B. Microhardness

Figure 9 shows the Vickers microhardness values along the cross-section of cladding layer and substrate. Hardness is significantly increased from 174 HV0.3 to 256 HV0.3 when traversed from the substrate to the top layer of the coating. The microhardness depth profile can be divided into three regions: cladding zone, Fe dilution zone, and substrate (Figure 8). The high hardness of the Inconel 625 cladding zone is attributed to the solid solution strengthening of the matrix phase by elements such as Mo and Nb. A small fraction of the secondary precipitates, i.e. the Laves phase, present in the interdendritic regions is also responsible for the high hardness values. The enhanced hardness at the top layer of the clad exists due to the fine equiaxed grains, which were evolved by higher cooling rate due to the direct exposure to the surrounding air. The decrease in microhardness in the Fe dilution zone is attributed to the element composition change due to the diffusion of iron by partial dilution from substrate to coating. The clad hardness decreases with increasing Fe dilution [24].

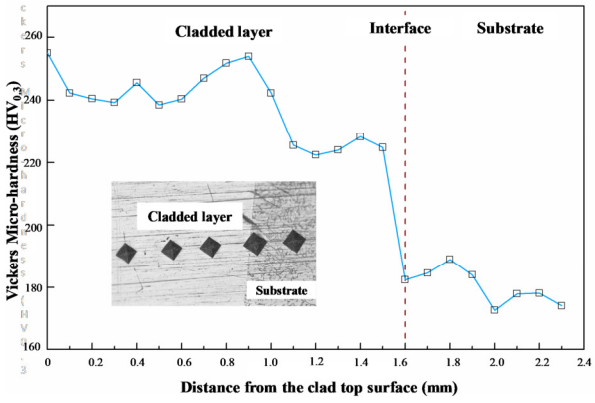

Fig. 8. Vickers microhardness profile obtained for the Inconel 625 laser cladded sample.

IV. CONCLUSION

In the present work, defect-free laser cladding coatings were fabricated on the surface of AISI 304 stainless steel samples using Inconel 625 powder deposition. The solidification microstructures, compositions, phases formed, and microhardness of the coating and bonding regions were investigated. Laser cladding exhibited a good metallurgical bonding between the substrate and the coating. The morphology of the grains varied from the bonding region to the top layer of the clad in the following fashion: planar, cellular, columnar dendritic, and equiaxed crystals. At the bottom region of coating, Fe dilution from the substrate to the coating was found. The indexing of diffraction pattern of Inconel 625 clad coatings showed that the coating consisted primarily of γ-Ni phase. The existence of a small Laves phase fraction was also detected. A maximum in microhardness appeared at the top zone of the clad coating, which is about 1.5 times higher than that of the stainless steel substrate. This indicates that the coated cladding sample may effectively resist the abrasive wear.

ACKNOWLEDGMENT

The authors would like to express their gratitude to Dr. Durga Prasad Muvva and Mr. Kumar Kanneboina, both technical assistants at BITS Pilani, K K Birla Goa Campus, for their assistance in the FESEM and XRD characterization.

REFERENCES

[1] M. A. Derakhshi, J. Kangazian, and M. Shamanian, "Electron beam welding of inconel 617 to AISI 310: Corrosion behavior of weld metal," *Vacuum*, vol. 161, pp. 371–374, Mar. 2019, https://doi.org/10.1016/j.vacuum.2019.01.005.

[2] M. Ramadan, "Interface Structure and Elements Diffusion of As-Cast and Annealed Ductile Iron/Stainless Steel Bimetal Castings," *Engineering, Technology & Applied Science Research*, vol. 8, no. 2, pp. 2709–2714, Apr. 2018, https://doi.org/10.48084/etasr.1856.

[3] A. S. C. M. D'Oliveira, P. S. C. P. da Silva, and R. M. C. Vilar, "Microstructural features of consecutive layers of Stellite 6 deposited by laser cladding," *Surface and Coatings Technology*, vol. 153, no. 2, pp. 203–209, Apr. 2002, https://doi.org/10.1016/S0257-8972(01)01687-5.

[4] J. C. Heigel, P. Michaleris, and T. A. Palmer, "In situ monitoring and characterization of distortion during laser cladding of Inconel® 625," *Journal of Materials Processing Technology*, vol. 220, pp. 135–145, Jun. 2015, https://doi.org/10.1016/j.jmatprotec.2014.12.029.

[5] J. del Val *et al.*, "Laser cladding of Co-based superalloy coatings: Comparative study between Nd:YAG laser and fibre laser," *Surface and Coatings Technology*, vol. 204, no. 12, pp. 1957–1961, Mar. 2010, https://doi.org/10.1016/j.surfcoat.2009.11.036.

[6] A. E. Pilehrood, A. Mashhuriazar, A. H. Baghdadi, Z. Sajuri, and H. Omidvar, "Effect of Laser Metal Deposition Parameters on the Characteristics of Stellite 6 Deposited Layers on Precipitation-Hardened Stainless Steel," *Materials*, vol. 14, no. 19, Jan. 2021, Art. no. 5662, https://doi.org/10.3390/ma14195662.

[7] Y. T. Xu, W. J. Zhao, T. D. Xia, and X. J. Wang, "Study of Laser Cladding Novel Co-9Al-7.5W Superalloy on 304 Stainless Steel," *Advanced Materials Research*, vol. 291–294, pp. 872–877, 2011, https://doi.org/10.4028/www.scientific.net/AMR.291-294.872.

[8] J. Pereira, J. Zambrano, M. Licausi, M. Tobar, and V. Amigó, "Tribology and high temperature friction wear behavior of MCrAlY laser cladding coatings on stainless steel," *Wear*, vol. 330–331, pp. 280–287, May 2015, https://doi.org/10.1016/j.wear.2015.01.048.

[9] J. C. Pereira, J. C. Zambrano, M. J. Tobar, A. Yañez, and V. Amigó, "High temperature oxidation behavior of laser cladding MCrAlY coatings on austenitic stainless steel," *Surface and Coatings Technology*, vol. 270, pp. 243–248, May 2015, https://doi.org/10.1016/j.surfcoat.2015.02.050.

[10] N. Jeyaprakash, C.-H. Yang, and S. Sivasankaran, "Laser cladding process of Cobalt and Nickel based hard-micron-layers on 316L-stainless-steel-substrate," *Materials and Manufacturing Processes*, vol. 35, no. 2, pp. 142–151, Jan. 2020, https://doi.org/10.1080/10426914.2019.1692354.

[11] E. R. I. Mahmoud and H. F. El-Labban, "Microstructure and Wear Behavior of TiC Coating Deposited on Spheroidized Graphite Cast Iron Using Laser Surfacing," *Engineering, Technology & Applied Science Research*, vol. 4, no. 5, pp. 696–701, Oct. 2014, https://doi.org/10.48084/etasr.483.

[12] M. T. Veiga, G. O. Verran, A. Rabelo, M. F. Teixeira, P. R. A. Bloemer, and L. J. da Silva, "Laser cladding of a cobalt-based superalloy on austenitic stainless steel," *Soldagem e Inspecao*, vol. 26, 2021, https://doi.org/10.1590/0104-9224/SI26.02.

[13] G. Muvvala, D. Patra Karmakar, and A. K. Nath, "Online monitoring of thermo-cycles and its correlation with microstructure in laser cladding of nickel based super alloy," *Optics and Lasers in Engineering*, vol. 88, pp. 139–152, Jan. 2017, https://doi.org/10.1016/j.optlaseng.2016.08.005.

[14] C. Li, Y. Xu, T. Jia, J. Zhao, and X. Han, "Numerical simulation research on multifield coupling evolution mechanism of IN625 laser cladding on nodular cast iron," *The International Journal of Advanced Manufacturing Technology*, vol. 119, no. 9, pp. 5647–5669, Apr. 2022, https://doi.org/10.1007/s00170-021-08249-y.

[15] K. Touileb, R. Djoudjou, and A. Ouis, "Effect of Viscosity on the GTA Welds Bead Penetration in Relation with Surface Tension Elements," *Engineering, Technology & Applied Science Research*, vol. 6, no. 2, pp. 952–955, Apr. 2016, https://doi.org/10.48084/etasr.643.

[16] N. A. Berjeza, S. P. Velikevitch, V. I. Mazhukin, I. Smurov, and G. Flamant, "Influence of temperature gradient to solidification velocity ratio on the structure transformation in pulsed- and CW-laser surface treatment," *Applied Surface Science*, vol. 86, no. 1, pp. 303–309, Feb. 1995, https://doi.org/10.1016/0169-4332(94)00446-3.

[17] B. Fotovvati, S. F. Wayne, G. Lewis, and E. Asadi, "A Review on Melt-Pool Characteristics in Laser Welding of Metals," *Advances in Materials Science and Engineering*, vol. 2018, Apr. 2018, Art. no. e4920718, https://doi.org/10.1155/2018/4920718.

[18] M. Xiaoli, W. Kaiming, F. Hanguang, J. Jiang, L. Yongping, and Y. Dawei, "Effect of mo Content on Microstructure and Properties of Laser Cladding Fe-BASED Alloy Coatings," *Surface Review and Letters*, vol. 25, pp. 1850077–168, Jan. 2018, https://doi.org/10.1142/S0218625X18500774.

[19] K. Feng *et al.*, "Improved high-temperature hardness and wear resistance of Inconel 625 coatings fabricated by laser cladding," *Journal of Materials Processing Technology*, vol. 243, pp. 82–91, May 2017, https://doi.org/10.1016/j.jmatprotec.2016.12.001.

[20] T. E. Abioye, D. G. McCartney, and A. T. Clare, "Laser cladding of Inconel 625 wire for corrosion protection," *Journal of Materials Processing Technology*, vol. 217, pp. 232–240, Mar. 2015, https://doi.org/10.1016/j.jmatprotec.2014.10.024.

[21] D. Deng, in *Additively Manufactured Inconel 718 : Microstructures and Mechanical Properties*, Linköping, Sweden: Linköping University Electronic Press, 2018, pp. 12–13.

[22] S. G. K. Manikandan, D. Sivakumar, K. Prasad Rao, and M. Kamaraj, "Laves phase in alloy 718 fusion zone — microscopic and calorimetric studies," *Materials Characterization*, vol. 100, pp. 192–206, Feb. 2015, https://doi.org/10.1016/j.matchar.2014.11.035.

[23] S. Antonov *et al.*, "The effect of phosphorus on the formation of grain boundary laves phase in high-refractory content Ni-based superalloys," *Scripta Materialia*, vol. 161, pp. 44–48, Mar. 2019, https://doi.org/10.1016/j.scriptamat.2018.10.015.

[24] S. Zanzarin, S. Bengtsson, and A. Molinari, "Study of dilution in laser cladding of a carbon steel substrate with Co alloy powders," *Powder Metallurgy*, vol. 59, no. 1, pp. 85–94, Jan. 2016, https://doi.org/10.1080/00325899.2015.1118842.